A Silicate Inclusion in Puente del Zacate, a IIIA Iron Meteorite

Edward J. Olsen, Andrew M. Davis, Robert N. Clayton, Toshiko K. Mayeda, Carleton B. Moore, Ian M. Steele

The IIIA and IIIB iron meteorites are considered to have formed in the cores of asteroids. A silicate inclusion within the IIIA meteorite Puente del Zacate consisting of olivine (Fa_4), low-calcium pyroxene (Fs_6Wo_1), chromium diopside (Fs_3Wo_{47}), plagioclase ($An_{14}Or_4$), graphite, troilite, chromite, daubreelite, and iron metal resembles inclusions in IAB iron meteorites. The oxygen isotopic composition of the Puente del Zacate inclusion is like chromite and phosphate inclusions in other IIIA and IIIB irons. The Puente del Zacate inclusion may have been derived from the lower mantle of the IIIAB parent asteroid.

We report here a study of a silicate inclusion in the IIIA iron meteorite Puente del Zacate (PDZ) (*1*). The IIIA (and the closely related IIIB) (*2*) iron meteorites are considered to have formed in the cores of asteroids. The IIIAB meteorites commonly contain small inclusions of chromite and one or more Fe-bearing phosphate minerals; the latter appear to have formed in situ at a late stage of core crystallization by oxidation of phosphorus alloyed in Fe-Ni metal (*3*). Mineralogical, chemical, and isotopic trends in silicate systems have revealed most of what is known about the evolution of asteroids. A silicate inclusion in PDZ provides more information about this major group of core-forming irons than can be gained from the dominant metallic phases alone.

The PDZ silicate inclusion is a 7-mm angular fragment within a troilite nodule measuring 16 mm in diameter (*4*). The inclusion has a granoblastic texture (*5*) with each silicate grain being 100 to 200 μm in its largest dimension. One portion of the section, measuring 1500 μm by 500 μm, consists of a compact silicate mass containing minor grains of troilite, chromite, and Fe-Ni metal (Fig. 1). Most of the section's area, however, is riddled with small cavities (Fig. 1). Some cavities are filled with graphite; others are empty or have shreds of graphite along their edges. We shall assume that the empty and nearly empty cavities were once filled with graphite that, being a soft mineral, was torn out during the original sawing of the meteorite that exposed the inclusion. The silicates were analyzed with the use of an electron microprobe (*6*) (Table 1), revealing olivine (Fa_4), low-Ca pyroxene (Fs_6Wo_1), chromium diopside (Fs_3Wo_{47}), and plagioclase ($An_{14}Or_4$). The silicates are unzoned and show no significant grain-to-grain compositional variations. In addition to graphite, the inclusion contains minor amounts of troilite, chromite, daubreelite, and Fe-Ni metal; no phosphate minerals were found. Optical point counting of silicates was problematic because it was difficult to discriminate between the two pyroxenes and olivine on the thick, polished section. A point count, however, did indicate that the section consists of about 25 weight % graphite (or cavities). The electron microprobe was used to determine a bulk composition, assuming the area of the section is representative of the whole rock (*7*) (Table 1). From the bulk analysis and the individual silicate mineral analyses, a mode was calculated (values in weight percent; relative error, ±10%): olivine, 23; low-Ca pyroxene, 14; chromium diopside, 15; plagioclase, 15; troilite, 1; graphite, 27; chromite, 0.5; and metal, 4.

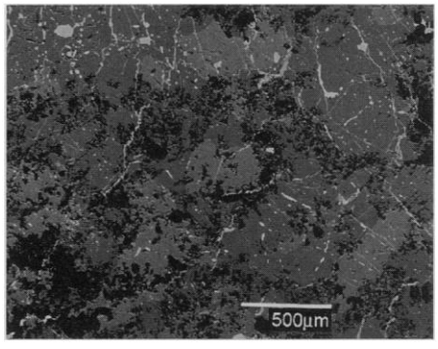

Fig. 1. Backscattered electron image of a portion of the PDZ silicate inclusion. The lightest shade of gray is chromium diopside. The darker shade of gray is olivine, low-Ca pyroxene, and plagioclase, all of which have similar mean atomic numbers. The black areas are graphite or cavities that were once filled with graphite. The bright white areas are troilite, chromite, Fe-Ni metal, or daubreelite.

Ion microprobe analyses (*8*) were conducted to identify rare earth elements (REEs) on individual silicate grains. Combined with the calculated mode, the whole-rock REE pattern was calculated (Fig. 2). The REE pattern, normalized to Type 1 carbonaceous chondrites (C1) (*9*), is, within errors, essentially flat at about 2.5× enrichment.

The whole rock oxygen isotope composition ($\delta^{17}O$ = 1.15 per mil, $\delta^{18}O$ = 2.46 per mil) plots among the points for oxygen-bearing minerals (phosphates and chromites) in IIIAB irons (Fig. 3); together these lie along a chemical fractionation line that passes through whole rock points for silicates in stony iron pallasites and mesosiderites (*10*) and basaltic achondrites (*11*, *12*).

The petrography, mineralogy, and respective silicate mineral compositions of the PDZ inclusion are similar to silicate inclusions found in the group of iron meteorites called IAB (*13*). Some IAB silicate inclusions (Odessa type) have granoblastic textures. Silicate minerals in IAB inclusions have small differences in composition from one IAB meteorite to another but no zoning or grain-to-grain compositional variations within individual meteorites. The inclusions of PDZ and IAB have the same degree of reduction as measured by the FeO contents of the ferromagnesian minerals. These FeO contents are much lower than those of the same minerals in ordinary chondrites and HED achondrites but are higher than those of the extremely reduced minerals in the enstatite chondrites and enstatite achondrites. Graphite, intimately mixed with silicates, as in PDZ, is common in IAB inclusions.

Table 1. Electron microprobe analyses of PDZ inclusion and silicates. (A) PDZ whole rock. Each element has an estimated relative error of ±10% (*7*). (B) Chromium diopside (Fs_3Wo_{47}). (C) Olivine (Fa_4). (D) Low-Ca pyroxene (Fs_6Wo_1). (E) Plagioclase ($An_{14}Or_4$). Mineral phases: Fs, ferrosilite; Wo, wollastonite; Fa, fayalite; An, anorthite; Or, orthoclase.

Component	Composition (weight %)				
	A	B	C	D	E
SiO_2	36	54.36	42.44	59.66	65.29
Al_2O_3	3.4	0.89	0.00	0.00	21.46
Cr_2O_3	0.35	1.07	0.00	0.18	0.00
FeO	2.0	1.64	3.75	4.17	0.32
MnO	0.26	0.45	0.54	0.50	0.00
MgO	20	17.16	52.99	35.04	0.00
CaO	3.9	22.88	0.00	0.44	2.83
Na_2O	1.5	0.76	0.00	0.00	9.43
K_2O	0.10	0.00	0.00	0.00	0.67
FeS	1.2				
Fe	4.0				
C	27				
Total	99.45	99.21	99.72	99.99	100.00

E. J. Olsen and I. M. Steele, Department of the Geophysical Sciences, University of Chicago, Chicago, IL 60637, USA.
A. M. Davis and T. K. Mayeda, Enrico Fermi Institute, University of Chicago, Chicago, IL 60637, USA.
R. N. Clayton, Department of the Geophysical Sciences, Enrico Fermi Institute, and Department of Chemistry, University of Chicago, Chicago, IL 60637, USA.
C. B. Moore, Center for Meteorite Studies, Arizona State University, Tempe, AZ 85287, USA.

In spite of the similarity of the PDZ silicate inclusion to inclusions in some IAB irons, IIIAB irons and IAB irons themselves possess distinct differences. (i) The siderophile (*14*) trace-element compositions of IIIAB metal and IAB metal are distinct. Whereas siderophile trace-element trends indicate that IIIA and IIIB irons formed in cores, the trends in IAB irons indicate partial melting, incomplete segregation, and fractional crystallization. One interpretation of this difference is that IAB iron masses are not core irons but formed in pools on or near asteroid surfaces possibly as the result of impact melting events (*15*). Another interpretation asserts that IAB irons could have formed in cores as a result of low degrees of partial melting (*16*); this latter view is supported by the low cooling rates of IAB metal, 1° to 15°C per million years (*17*), rates that are too low to reconcile with a near-surface origin. (ii) Oxygen isotopic compositions of oxygen-bearing minerals in IIIAB irons are distinct from those in IAB irons (*12*) (Fig. 3), leading to the conclusion that IIIAB and IAB irons come from separate parent asteroids. (iii) IIIAB metal contains ≤0.1 weight % carbon; PDZ has only 0.01 to 0.05 weight % carbon (*18*). IAB irons contain 0.2 to 2 weight % carbon (*18*) alloyed in metal, sometimes in cohenite (*19*) and often as graphite inclusions. With the low bulk carbon content of PDZ, it is extraordinary to find graphite in this IIIA iron.

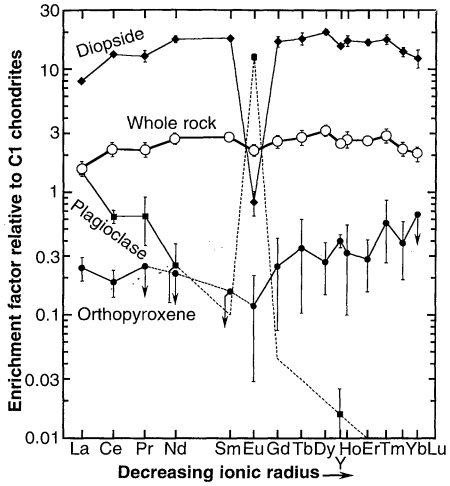

Fig. 2. Enrichment factors (relative to C1 chondrites) of REEs and yttrium (which chemically functions like the REEs) measured in PDZ silicates and calculated for the whole rock.

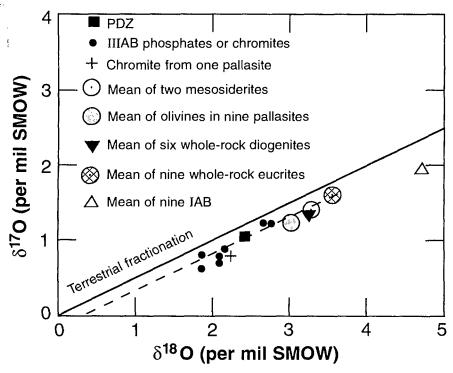

Fig. 3. The oxygen isotope composition of whole-rock PDZ plots among oxygen-bearing phases of IIIAB iron meteorites, which lie on an isotopic chemical fractionation line (dashed line) that includes pallasites, mesosiderites, and the basaltic achondrites. A mean value for silicates in nine IAB irons is shown for comparison. The composition is measured relative to standard mean ocean water (SMOW).

It is difficult to account for the origin of the PDZ inclusion. The relatively flat bulk REE pattern (Fig. 2) suggests a chondritic source. The small enrichment (2.5 times that seen in C1 meteorites) is somewhat higher than that seen for the ordinary chondrites (1.4 times C1). Assuming that the REE pattern represents a whole rock (that is, not an unrepresentative fragment of a larger mass), the inclusion might be a product of a partial melting of a chondritic source, during which chemical reduction occurred. This is, however, unlikely because bulk REE patterns of ordinary chondrites are controlled to a significant extent by their phosphate minerals content (up to 1 weight %), phosphates being very enriched in REEs (from 10 times to over 100 times the C1 enrichment). A careful search of the PDZ inclusion, however, found no phosphate minerals. The REE pattern for PDZ was calculated from the pyroxenes and plagioclase phases only (20). The flat chondritic shape of the REE pattern in PDZ was acquired by some means other than derivation from a chondritic source.

The fractional crystallization of IIIAB metal is considered to have taken place in an asteroid core under an insulating silicate-rich mantle. How a graphite-bearing silicate inclusion was introduced into a low-carbon IIIA iron core is difficult to envision. Although the oxygen isotopic compositions of silicates in IAB irons indicate they did not occupy the same parent asteroid as IIIAB irons (*12*), the similarity of the PDZ inclusion to some IAB silicate inclusions suggests that the starting materials for each were more likely to be similar than different. If IIIAB irons do comprise asteroid cores, then the PDZ inclusion could have been derived from a reduced, differentiated lower mantle that has not been sampled as a separate meteorite type. The core-mantle interface of a IIIAB asteroid has usually been considered to be a pallasite (*10*) layer. The IIIA core could have sampled mantle rock if the pallasite layer was not uniformly present around the entire core. Another possibility is that some IIIAB irons did not form in core positions but as separate smaller masses within the mantle, where thermal insulation was sufficient to allow slow fractional crystallization, giving them the fractionated siderophile trace-element signature of core irons but putting them into contact with mantle rocks of types not yet known as separate meteorites. If IAB irons are actually core irons (*16, 17*), their frequent association with silicate inclusions similar to the PDZ inclusion suggests that the IIIAB mantle mineralogy could be similar to IAB mantle mineralogy. The major difference between these two kinds of core iron would then be only a matter of the degree of partial melting that took place in the respective cores: IIIAB cores represent a high degree of melting followed by slow fractional crystallization, whereas IAB cores represent low and variable degrees of partial melting, yielding core metal that is less uniform, displaying incomplete fractional crystallization.

REFERENCES AND NOTES

1. Arizona State University specimen 94b. The IIIA classification of a metal sample collected from this specimen was confirmed by J. T. Wasson of the University of California, Los Angeles. Composition (in parts per million): Ga, 19; As, 4.8; and Ir, 1.2.
2. Collectively called IIIAB.
3. E. Olsen and K. Fredriksson, *Geochim. Cosmochim. Acta* **30**, 459 (1966); E. Olsen and I. Steele, *Meteoritics* **28**, 415 (1993); *Lunar Planet. Sci.* **XXV**, 1025 (1994).
4. To preserve this scarce material, we performed the entire study on a 4 mm by 4 mm chip from an exposed saw-cut surface, prepared as a polished (thick) section, and from a small chip removed for oxygen isotope analysis. No thin section was made because that would have caused loss of material and reduced the section's area.
5. Granoblastic texture consists of approximately equidimensional crystals with well-sutured boundaries.
6. Analyses were performed on a Cameca SX-50 electron probe microanalyzer (15 kV, 25 nA); we analyzed natural and synthetic standards with online PAP corrections.
7. We analyzed 309 scanned areas each measuring 100 μm on a side. This size area violates the electron beam geometry used to calculate the standard analytical corrections. To estimate the error, we analyzed several such areas covering monomineralic silicate phases; the relative errors were within ±10% for each element for the same minerals analyzed by a 2-μm-spot beam. The 309 analyses covered about one-fourth of the section's area. Many analyses gave low totals because of cavities or graphite (the instrument does not detect carbon). The averaged results gave 27 weight % pore space, in good agreement with the point count; we shall assume that this percentage represents original graphite. The whole-rock analysis in Table 1 used the averaged values of the 309 analyses, an average that could vary relatively by ±10% for each element analyzed.
8. Ion microprobe data were collected with an Associated Electrical Industries (AEI) IM-20 ion microprobe using magnetic peak switching at low mass resolution ($M/\Delta M$ = 500). Molecular interferences were suppressed by energy filtering. Calcium-normalized ion yields and interferences were determined from a variety of silicate minerals and glasses. E. Zinner and G. Crozaz, *Int. J. Mass Spectrom. Ion Processes* **69**, 17 (1986).

9. Chondrites are primitive meteorites that contain small spherules, called chondrules, and appear to have been produced very early in the formation of the solar system. The C1 chondrites are the most primitive, and chemical data are commonly normalized to their composition.
10. Pallasites and mesosiderites are stony iron meteorites consisting of silicate masses contained in a matrix of Fe-Ni metal. Pallasites are considered to have comprised the boundary between the core and the mantle of asteroid bodies.
11. Basaltic achondrites (collectively called HED) are stony meteorites that have undergone complex igneous histories; eucrites bear a resemblance to terrestrial basalt lavas.
12. R. Clayton, *Annu. Rev. Earth Planet. Sci.* **21**, 115 (1993).
13. T. Bunch *et al.*, *Contrib. Mineral. Petrol.* **25**, 297 (1970).
14. Siderophile elements are those that alloy in Fe-Ni metal.
15. B.-G. Choi *et al.*, *Geochim. Cosmochim. Acta* **59**, 593 (1995).
16. A. Kracher, *Proc. Lunar Planet. Sci. Conf.* **15**, C689 (1985).
17. A. Meibom *et al.*, *Meteoritics* **30**, 544 (1995).
18. V. F. Buchwald, *Handbook of Iron Meteorites* (Univ. of California Press, Berkeley, 1975).
19. Cohenite is an Fe-Ni carbide mineral.
20. The REE content of olivine is so low that its contribution to the whole rock composition is negligible.
21. We thank J. T. Wasson for analyzing this PDZ metal to confirm its IIIA classification, E. R. D. Scott for a helpful discussion, R. Schmitt for a noble attempt to analyze a vanishingly small flake of PDZ, and two anonymous referees who added stimulating ideas and improved this report immeasurably. This work was supported by NASA grants NAGW-3569 (E.J.O.), NAGW-3384 (A.M.D.), and NAGW 3416 (I.M.S.) and NSF grants EAR 92-18857 (R.N.C.), EAR-9303530 (I.M.S.), and EAR-9316062 (I.M.S.).

21 May 1996; accepted 18 July 1996

Radiocarbon in Hydrologic Systems Containing Dissolved Magmatic Carbon Dioxide

Timothy P. Rose* and M. Lee Davisson

In regions of active volcanism, the presence of magmatic carbon dioxide (CO_2) in regional hydrologic systems provides a radiocarbon-depleted tracer for delineating ground-water transport and mixing processes and provides a means of assessing regional magmatic carbon fluxes. Variations in the stable carbon isotopic composition ($\delta^{13}C$) and carbon-14 values of springs and surface waters from the southern Cascade Range show consistent patterns of carbon isotopic mixing between magmatic, biogenic, and atmospheric CO_2 reservoirs. Radiocarbon measurements of waters from the Lassen region in northern California were used to construct a ground-water carbon-14 contour map, revealing principal subsurface flow paths and a broad region of diffuse magmatic CO_2 flux.

Recent soil gas studies have shown that large quantities of magmatic CO_2 are released as diffuse emissions from the flanks of some active volcanoes (*1*). In many cases, the CO_2 must percolate through a thick section of water-saturated bedrock on its way to the surface, raising the question of how much of the total CO_2 flux is removed by dissolution in ground water. If the quantity of dissolved CO_2 is characteristically large relative to the diffuse or geothermal gas flux, it may have implications for estimates of the global volcanic CO_2 flux (*2*) or studies of catastrophic CO_2-degassing events (*3*). Because magmatic CO_2 ordinarily contains no ^{14}C, the measurement of ground-water ^{14}C activities in volcanically active regions may provide a means of addressing this question. We describe here results from a regional ^{14}C hydrologic survey in the southern Cascade Range of California and Oregon.

We collected about 40 water samples from springs and spring-fed creeks in the southern Cascades during 1994 and 1995, more than half of which were from the Lassen region (Fig. 1). Dissolved inorganic carbon (DIC) extracted from these samples (*4*) was analyzed for ^{14}C and $\delta^{13}C$ (*5*). Graphical variations in ^{14}C versus $\delta^{13}C$ values (Figs. 2 and 3) reveal similar isotope mixing patterns in each volcanic system. We identified three DIC end members, with isotopic compositions represented in Fig. 2 by shaded boxes: (i) DIC in equilibrium with biogenic soil CO_2 [with $\delta^{13}C_{DIC}$ near -18 per mil relative to the Pee Dee belemnite (PDB) standard and $^{14}C \geq 100\%$ modern carbon (PMC)]; (ii) DIC in equilibrium with atmospheric CO_2 [$\delta^{13}C_{DIC}$ near 0 per mil, $^{14}C \geq 100$ PMC]; and (iii) DIC in equilibrium with magmatic CO_2 [$^{14}C = 0$ PMC]. Carbonate rock is absent in the study areas.

Dissolved inorganic carbon of magmatic origin can show a range in $\delta^{13}C$ values that depends on the initial composition of the CO_2 gas and on the temperature and pH conditions during CO_2-DIC equilibration (*6*). In the Lassen region, magmatic DIC–enriched fluids (with $^{14}C \leq 1$ PMC) were observed only in bicarbonate (HCO_3^-) hot springs (temperature $T = 60°$ to 80°C; pH = 6.4). The $\delta^{13}C$ values of these springs (-5.7 to -7.0 per mil) are consistent with the results that would be obtained as a result of high-temperature isotopic equilibration with CO_2 gas from the Lassen geothermal system ($\delta^{13}C = -7.5$ to -10.5 per mil; average value $= -9.5$ per mil) (*7*). Lower temperature (10°C) equilibration with Lassen geothermal CO_2 could yield $\delta^{13}C_{DIC}$ values as enriched as 0 per mil (shaded box in Fig. 2).

At other Cascade volcanic centers, fluids with negligible ^{14}C activity were observed only in low-temperature, CO_2-rich soda springs (*8*). Soda spring $\delta^{13}C$ values ranged from -11.7 to -7.3 per mil and showed an increase in pH from 4.5 to 6.4 that is concomitant with increasing $\delta^{13}C$ values (Fig. 3).

The $\delta^{13}C$-^{14}C data from the Lassen region define three distinct mixing arrays, represented by linear trends in Fig. 2, all with a common origin at the biogenic DIC end member. Large springs (flow > 0.3 m^3 s^{-1}) generally have lower ^{14}C values relative to smaller springs, implying a deeper, regional ground-water flow path (*9*) with a higher probability for interaction with magmatic CO_2. Simple mixing of ground waters containing biogenic DIC with waters similar in composition to the HCO_3^- hot springs produced the "dead carbon addition" mixing line of Fig. 2. The exceptional linearity of the data along this trend suggests mixing with magmatic DIC equilibrated over a limited range of temperature and pH conditions.

A second mixing line in Fig. 2 is defined by the interaction of waters containing biogenic DIC with waters that recharge in the Lassen Peak region. The latter is characterized by surface water from Lost Creek, which originates from springs on the poorly vegetated north slope of Lassen Peak and has a $\delta^{13}C$ value that indicates low-temperature equilibration with a mixture of magmatic and atmospheric CO_2 gases. Winter snowfall in this region averages >2.3 m of

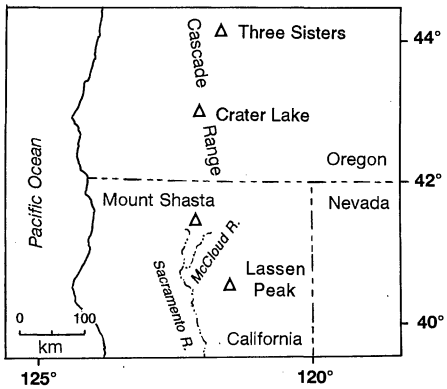

Fig. 1. Map showing locations of major volcanic centers and rivers discussed in the text.

Isotope Sciences Division, L-231, Lawrence Livermore National Laboratory, Livermore, CA 94550, USA.

*To whom correspondence should be addressed.